Assessment of hydride precipitation modelling across fuel cladding: Hydriding in non-defective and defective fuel rods

F. Feria [*], L.E. Herranz

Unit of Nuclear Safety Research, CIEMAT, Avda. Complutense 40, 28040 Madrid, Spain

A B S T R A C T

This work studies the effect of the hydrogen precipitation on the in-clad hydrides distribution, given its potential impact on cladding integrity (ductility reduction). To do so, a hydrogen migration/precipitation model derived, called HYDCLAD, has been extended to take into account two different options for the precipitation modelling: a semi-empirical approach and a more phenomenological one. The model has been further extended to encompass the variability of existing solubility limits.

Different scenarios of hydrogen uptake have been assessed from non-defective and defective irradiated fuel rods. In the first case, the comparison with data allows concluding that the more phenomenological approach better predicts the hydride rim if a re-parameterization is done along with the oxidation front effect modelled in HYDCLAD. In defective fuel rod, the enhancement with the more phenomenological approach is capable of estimating the hydrides blisters expected under massive hydrogen uptake in the cladding fuel side. The variability of the solubility limits hardly has an impact on hydrides distribution.

1. Introduction

The diffusion and precipitation of the hydrogen picked up in LWR fuel claddings is a key aspect for fuel safety given its impact on the material resistance to failure. The hydriding of Zircaloy claddings may give rise to the formation of dense hydrides regions, which notably reduces the alloy ductility. At high burnup, the so-called hydride rim is related to the formation of a much higher hydrogen concentration close to the cladding water side (Nagase and Uetsuka, 1997). In the particular case of defective fuel rods, hydrogen can be picked up in the cladding fuel side (secondary hydriding), which may lead to a massive hydriding that may evolve into the formation of hydrides blisters (Evdokimov et al., 2011; Lee et al., 2017).

To predict the consequences of the hydriding it is of utmost interest to properly model the in-clad hydrogen migration and precipitation. In other words, the estimation of the extension and concentration of the hydrides formed is needed to characterise the mechanical state of the cladding. This is especially important if transient mechanical loads would come into play after the hydriding (i.e., conditions that would lead to cladding failure).

The experimentation and modelling of in-clad hydrogen performance mechanisms have been an object of study over the years (Sawatzky, 1960;

Kearns, 1967; Marino, 1972; Kammenzind et al., 1997; McMinn et al., 2000; Une et al., 2009; Courty et al., 2014; Courty et al., 2015; Passelaigue et al., 2021a). This has allowed enhancing the predictability of fuel performance codes. So far, the main focus of interest has been the behaviour of the hydrogen picked up in the cladding water side, which is currently modelled in codes like BISON (Stafford, 2015), SVECHA/QUENCH (Veshchunov et al., 2016), TESPA-ROD (Sonnenburg and Boldt, 2017) or FRAPCON-xt (Feria and Herranz, 2018).

Current models encompass diffusion and thermo-diffusion as drivers of the atomic hydrogen migration, and precipitation of zirconium hydrides as a sink of the cited migration. The models derived so far require further validation to reduce uncertainties found (Stafford, 2015; Feria and Herranz, 2018; Passelaigue et al., 2022). In particular, hydrogen precipitation needs further research. Earlier modelling is based on the fact that there is hysteresis in the solubility limit (i.e., precipitation and dissolution limits) and the precipitation kinetics are independent of the hydrides formed (Courty et al., 2014; Stafford, 2015). However, recent studies suggest that there is only one thermodynamic solubility limit with precipitation kinetics depending on hydrides present in the cladding, from which a new model has been derived (Passelaigue et al., 2021a); recently, this model has been updated taking into account non-fixed solubility limits along time (Passelaigue et al., 2022). This latest

---

approaches, though, should be validated against representative data from irradiated fuel rods.

This work studies the effect of the hydrogen precipitation modelling on the in-clad hydrides distribution when simulating both separate effect tests and integral scenarios representative of PWR conditions with intact and defective fuel rods. This activity has been carried out in the framework of the R2CA project (within Work Package 4). The study has been performed with HYDCLAD, the in-clad hydrogen model built-up (Feria and Herranz, 2018), which latest developments are also described in this paper. HYDCLAD extensions involve three different aspects: an additional precipitation model has been implemented based on Passelaigue et al. (2022); based on the variability of the solubility limits reported in the literature (Zanellato et al., 2012), several options have been included to enable sensitivity analyses; and, finally, model application to fuel side hydrogen uptake (i.e., defective fuel rods) has been made possible.

2. HYDCLAD model

2.1. Fundamentals

HYDCLAD is a 1D model of the hydrogen performance across the cladding thickness derived by CIEMAT (Feria and Herranz, 2018; Feria et al., 2020b). The fundamentals for modelling diffusion and precipitation/dissolution phenomena, as well as the initial and boundary conditions are described below.

2.1.1. Diffusion

The general equation used to model the diffusion of the hydrogen concentration, H, is based on the Fick's second law. Focusing on the radial direction, r, it is expressed as:

$$\frac{dH}{dt} = -\frac{dJ}{dr} \tag{1}$$

where H is the hydrogen concentration, J the hydrogen flux and r the radial direction. The hydrogen flux is calculated taking into account both the concentration gradient (Fick's first law) and the temperature gradient (Soret's law):

$$J = -D\left(\frac{dH}{dr} + \frac{Q^* \cdot H}{RT^2}\frac{dT}{dr}\right) \tag{2}$$

where D is the diffusion coefficient, Q^* the heat of transport, T the temperature and R the ideal gas constant. The hydrogen concentration is split into dissolved, H_d, and precipitated, H_p, based on the solubility limits, as is shown in the following section. In order to consider the mass transfer through a two phase-region, the volume fraction of the hydride phase, f, is accounted for. It is determined through the ratio between H_p and the local concentration of hydrogen in hydride precipitates, $H\delta$. The details of D, Q^* and $H\delta$ are reported elsewhere (Stafford, 2015; Veshchunov et al., 2016). It should be mentioned that the modelling of the hydrogen mobility and hydride orientation related to the stress (Bruni et al., 2011; Massih and Jernkvist, 2009) is not taken into account under irradiation conditions.

2.1.2. Precipitation/dissolution

The classic modelling of hydrogen precipitation/dissolution in the zirconium alloy is used, based on empirical terminal solid solubilities concerning precipitation (TSS_p) and dissolution (TSS_d), assuming that there is hysteresis (Courty et al., 2014). The calculation of the precipitation rate is based on the linear approximation in the hydride precipitation model (Marino, 1972); concretely, the rate of precipitation was measured to be proportional to the hydrogen supersaturation. If the concentration in solid solution lies between TSS_p and TSS_d (i.e., hysteresis area), neither dissolution nor precipitation occurs. When the concentration in solid solution is below the TSS_d, there is only a change

in the precipitation rate if hydrides are present (i.e., dissolution of the hydrides). Therefore, the precipitation rate is determined from TSS_p, TSS_d and the precipitation and dissolution rate parameters (k_p and k_d, respectively):

$$\frac{dH_p}{dt} = \begin{cases} k_p \cdot (H_d - TSS_p) & \text{if } H_d > TSS_p \\ 0 & \text{if } TSS_p \geqslant H_d > TSS_d \\ k_d \cdot (H_d - TSS_d) & \text{if } H_d \leqslant TSS_d \text{ and } H_p > 0 \\ 0 & \text{if } H_d \leqslant TSS_d \text{ and } H_p = 0 \end{cases} \tag{3}$$

The details of the kinetic parameters and the solubility limits are shown elsewhere (Stafford, 2015; Veshchunov et al., 2016). The options used by default in HYDCLAD are depicted in Figs. 1 and 2, respectively (represented as blue lines).

Additionally, CIEMAT implemented an additional contribution to the hydrogen migration/precipitation based on the effect of the oxidation front (Feria and Herranz, 2018). Particularly, from experimental observations made by Tupin et al. (2015), it is modelled that the hydrogen from the hydrides incorporated in the oxide is pushed ahead of the oxidation front, which implies inwards transport into the most external location of the metallic cladding and its subsequent reprecipitation. The latter is simulated through a fitting parameter, rp, with a value between 0 (instantaneous reprecipitation) and 1 (reprecipitation according to the kinetics modelled), given the lack of data concerning the effect of hydrides in the reprecipitation kinetics.

Accordingly, the precipitation rate is re-casted as,

$$\frac{dH_p}{dt} = \frac{dH_{p0}}{dt} - rp \cdot \frac{dH_{ox}}{dt} \tag{4}$$

where H_{p0} is the precipitated hydrogen obtained from equation (3) (i.e., without the effect of the oxidation front), H_{ox} is the concentration of precipitated hydrogen covered by the oxidation front, and rp is the fraction of H_{ox} that does not re-precipitate instantaneously (the reprecipitation kinetics has been modelled by the same k_p as the precipitation).

The assessment against post-irradiation measurements of a high burnup fuel rod showed that this contribution with rp values close to 1 considerably enhances the prediction of the hydride rim (Feria and Herranz, 2018), so this is the value adopted by default.

2.1.3. Initial and boundary conditions

The initial conditions for HYDCLAD (i.e., as-fabricated cladding thickness and hydrogen concentration), as well as the time step, the number of in-clad radial nodes and the fuel rod axial node simulated, are given through an input file, while the boundary conditions (i.e., hydrogen pickup, H_{pk}, oxide thickness, δ_{ox}, and thermal conditions; steady-state and transient conditions can be applied) can be provided through the input or by the coupling with a fuel performance code. Particularly, the model is prepared to be coupled with the FRAPCON code (version 4.0) (Geelhood et al., 2015).

The hydrogen pickup provided by FRAPCON is used as the boundary condition in the waterside node and the oxide thickness given by the code is used for the above mentioned oxidation front modelling. Concerning the thermal conditions, FRAPCON calculates the inner and outer cladding temperature (it does not nodalize the cladding thickness), from which HYDCLAD estimates the thermal gradient in the nodes established; particularly, a linear interpolation is assumed.

It should be noted that the model is solved by the numeric method of finite differences. The method is stable if $\Delta t \leq \Delta r / 2 \cdot D_{max}$, where Δt and Δr are the temporal and spatial discretization steps, respectively, and D_{max} the maximum value of the diffusion coefficient.

2.2. Extension

In this work, HYDCLAD has been extended to account for a new approach for precipitation/dissolution modelling, as an alternative option to the previous approach. Moreover, the model has been also
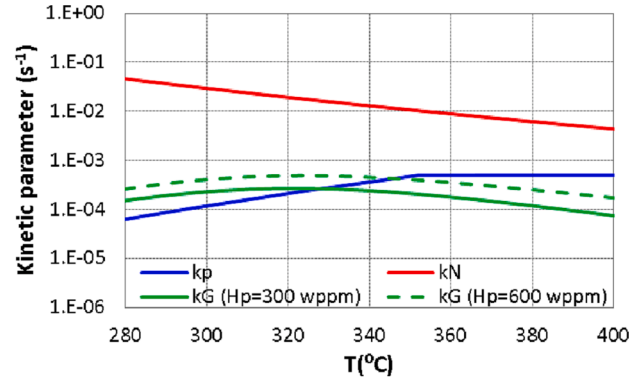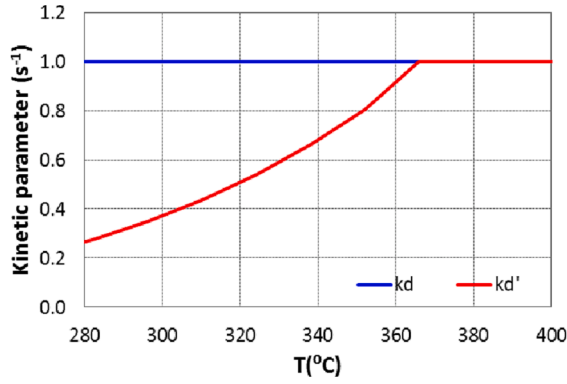
Fig. 1. Kinetic parameters for dissolution (left) and precipitation (right, with y-axis in logarithmic scale) as a function of temperature.
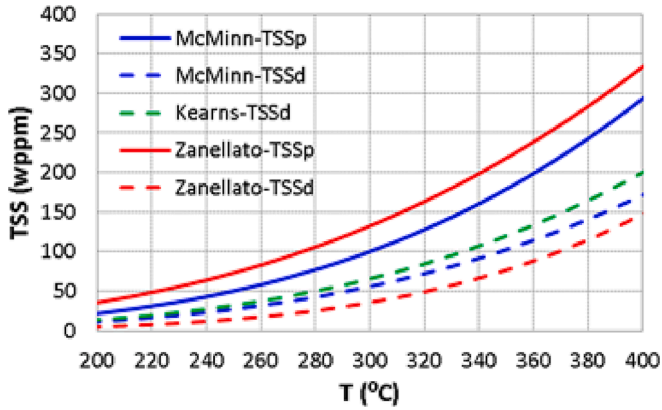

Fig. 2. TSS curves implemented in HYDCLAD.

extended with additional options of solubility limits experimentally found. Concerning the boundary conditions, the model has been adapted to take into account the fuel side hydrogen uptake under secondary hydriding scenarios. These extensions are described below.

2.2.1. Precipitation/dissolution

A new model for precipitation/dissolution proposed by Passelaigue et al. (2021a), called Hydride Nucleation-Growth-Dissolution (HNGD), has been implemented in HYDCLAD. In this model, hydride precipitation is divided into nucleation of new hydrides and growth of existing ones. Nucleation and growth of new hydrides occur when the dissolved hydrogen is above the TSS_p, which is identified as the supersolubility limit. The TSS_d is identified as the only thermodynamic solubility limit and the growth of existing hydrides occurs when the solid solution content is above. The kinetics of precipitation by hydride growth is described using the Johnson-Mehl-Avram-Kolmogorov model (Avrami, 1939).

The equations describing this model are the following:

where k_d', k_N and k_G are the kinetic parameters for dissolution, nucleation and growth, respectively, which are function of the temperature (k_G also depends on the precipitated hydrides, related to the effect of local stress on the diffusion around the hydrides), x is a measure of the advancement of the precipitation reaction and p is the dimensionality of the growth. The details of the model's parameters are given in Passelaigue et al. (2021a).

In order to compare the kinetic parameters of this new approach with the ones of the previous approach (i.e., classic modelling shown in equation (3) of section 2.1.2), Fig. 1 illustrates the evolution of these parameters with temperature. Different trends with temperature are observed regarding the modelling of each parameter for dissolution and precipitation. This should be explained by the experimental database that supports the modelling of each parameter, analysis of which is out of the scope of this work. Note that the kinetic parameter for nucleation used by the new modelling is several orders of magnitude greater than the kinetic parameter for precipitation used by the previous modelling. Considerably less difference can be observed with respect to the kinetic parameter for growth, even at the highest hydride content considered.

The approach described in the paragraphs above is hereafter referred as new approach with "static-TSSs".

Further extension of HYDCLAD has been done by implementing the latest HNGD model developments (Passelaigue et al., 2022). They imply adopting variable solubility limits (new approach with "dynamic-TSSs"):

"Effective supersolubility". Supersolubility is considered a variable value tending to the solubility value at long holds (i.e., matrix inhomogeneities may play a critical role in catalyzing nucleation). This gives rise to an effective supersolubility expressed as:

$$TSS_p^{eff} = TSS_p \ \ if \ \ \frac{\partial T}{\partial t} \neq 0$$

$$TSS_p^{eff} = TSS_d + (TSS_p - TSS_d) \cdot \exp\left(-\frac{t - t_0}{\tau}\right) \ \ if \ \ \frac{\partial T}{\partial t} = 0 \tag{6}$$

where t_0 is the time when the temperature hold starts and τ is the time parameter that characterizes the decrease.

$$\frac{dH_p}{dt} = \begin{cases} k_N \cdot (H_d - TSS_p) + k_G \cdot (H - TSS_d) \cdot p \cdot (1-x) \cdot (-\ln(1-x))^{1-1/p} & if \ H_d > TSS_p \\ k_G \cdot (H - TSS_d) \cdot p \cdot (1-x) \cdot (-\ln(1-x))^{1-1/p} & if \ TSS_p \geqslant H_d > TSS_d \\ k_d' \cdot (H_d - TSS_d) & if \ H_d \leqslant TSS_d \ and \ H_p > 0 \\ 0 & if \ H_d \leqslant TSS_d \ and \ H_p = 0 \end{cases} \tag{5}$$

"Growing solubility limit". Hydrides deform the matrix allowing accommodation of more hydrogen atoms in solution. Thus, the higher hydride concentration, the higher solubility limit. The corresponding effective solubility limit is given by:

$$TSS_d^{eff} = TSS_d + g \cdot v_\delta - ((1-\delta) \cdot TSS_d + g) \cdot v_\delta^2 \qquad (7)$$

where $v\delta$ is the hydride volume fraction and g and δ are fitting parameters. All these parameters are detailed in Passelaigue et al. (2022). In case of g, it is related to the increase in hydrogen solubility caused by the previous precipitation of hydrides (important in case of low hydride content); concerning the parameter δ, it is the fraction of the unmodified solubility in a solid hydride (relevant for high hydride content).

This modelling has been assessed against out-of-pile experiments by Passelaigue et al. (2021b), through which the parameters that better fit to the data have been given: $\tau = 10^4$ s, $\delta = 1.05$ and $g = 120$ wppm (new approach with "static-TSSs" corresponds to $\delta = 1$, $g = 0$ wppm and a τ value far higher than the time of the case simulated). It should be noted that this new modelling used in this work is based on assumptions (controlled through the above mentioned parameters) that need further analysis. Indeed, this modelling has not been validated against in-reactor data.

Concerning the TSSs, given the variability found in Zanellato et al. (2012), alternative options to the ones considered by default in HYDCLAD (McMinn et al., 2000) have been added to the model. Particularly, the correlations given by Kearns (1967) (for TSS_d) and Zanellato et al. (2012) (for TSS_d and TSS_p) have been implemented. Fig. 2 depicts the TSSs taken into account in the model. As it can be seen from the curves represented, the variability is not negligible; indeed, comparing McMinn's with Zanellato's curves at 300 °C, relative deviations greater than 30% have been found.

2.2.2. Boundary conditions

The CIEMATs model has been also adapted to account for a hydrogen pickup fraction under massive hydrogen uptake in the cladding fuel side, as an additional boundary condition related to the secondary hydriding in defective fuel rods.

For the assessment aimed at this work (focused on hydrides redistribution within the cladding), an ad-hoc hydrogen pickup fraction has been implemented in HYDCLAD, supported on a database from an experimental program at the Centre for Energy Research (EK). This program consisted of experimental series with hydrogen charging of Zircaloy-4 cladding tube samples, reproducing massive hydrogen uptake. The tests covered the temperature range of 300–400 °C (typical cladding temperature range under normal operational conditions). The details of the experimental setup and the data obtained are shown elsewhere (Szabó and Hózer, 2019).

This adaptation of HYDCLAD has been done through the implementation of a correlation that reproduces the experimental data:

$$pk = 1 - \exp\left(-(A \cdot T + B) \cdot t^{(C \cdot T + D)}\right) \qquad (8)$$

with pk the hydrogen pickup fraction at each time t (expressed in hours) and T the cladding temperature (expressed in degrees Celsius). A, B, C and D are the fitting parameters (values shown in Table 1 for different temperature ranges); the correlation coefficient is 0.99. Fig. 3 shows the model-to-data comparison at 300 °C and 400 °C.

Note that in this case of massive hydrogen uptake in the cladding fuel side, the hydrogen content available to be picked up in the cladding is
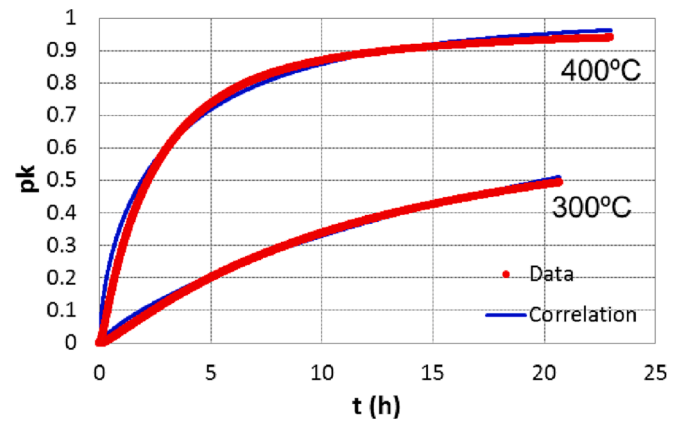

Fig. 3. Model-to-data comparison of hydrogen pickup fraction.

included as an additional input parameter of HYDCLAD, as well as the time at which the uptake starts. The coupling with FRAPCON still provides the irradiation conditions as the cladding temperature and the hydrogen uptake in the cladding water side. In the cladding fuel side it is assumed that the massive hydrogen uptake occurs without any oxide protective layer according to Lee et al. (2017) (in line with the EK experiment). In this regard, the above mentioned oxidation front effect contribution does not play any role in the simulation of the hydrogen uptake in the cladding fuel side.

3. Assessment

3.1. Scenarios

In this section, HYDCLAD model performance, particularly its updates and extensions (new approach for precipitation/dissolution, TSSs alternatives and secondary hydriding), has been tested in three scenarios:

- Out-of-pile thermal transients inducing successive hydrogen dissolution and precipitation (shown in section 3.2).
- In-reactor irradiation of a non-defective PWR fuel rod, which in-clad hydrogen distribution was characterized at the end of life (detailed in section 3.3.1).
- Postulated in-reactor secondary hydriding in a defective fuel rod with massive hydrogen uptake at the cladding fuel side (section 3.3.2). The lack of open data concerning in-clad hydrogen distribution on rods that underwent secondary hydriding turns this simulation into a performance consistency check.

The simulations carried out are classified according to the precipitation/dissolution modelling approach considered: previous approach (section 2.1.2) and new approach (section 2.2.1) both with "static-TSSs" and with "dynamic-TSSs". In the case of the previous approach and the new approach with "static-TSSs", default and alternative TSSs (shown in section 2.2.1) have been checked, while in the new approach with "dynamic-TSSs", parametric cases based on τ, δ, and g have been simulated:

- Fitting values to out-of-pile experiments (parametric called p0), as obtained by Passelaigue et al. (2022) ($\tau = 10^4$ s, $\delta = 1.05$ and $g = 120$ wppm).
- Bounding values (parametric called p1) of the ranges checked in Passelaigue et al. (2022) ($\tau = 10^{15}$ s, $\delta = 1.15$, and $g = 250$ wppm). It is worth noting that the τ value chosen is far longer than the cases duration.
- Values targeting the solubility limit parameter affecting high hydride content in the in-pile cases ($\delta = 1.15$ and $g = 0$ wppm), mentioned in
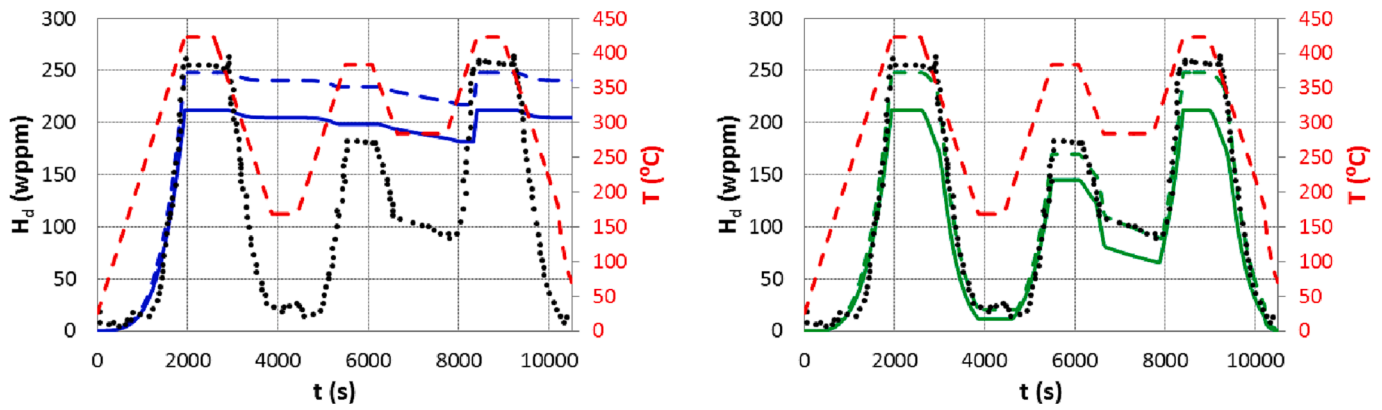
Table 1
Fitting parameters for hydrogen pickup correlation.

T	A	B	C	D
<330 °C	−0.0032	1.7512	0.0056	−1.6092
330 °C ≤ T < 370 °C	−0.0055	2.5072	0.0083	−2.5122
≥370 °C	0.0048	−1.2946	−0.0034	1.8055

Fig. 4. Evolution during the simulated experiment of the temperature (red dashed line) and the dissolved hydrogen, both measured (black dots) and predicted with the previous modelling (left) and with the new modelling with "static-TSSs" (right), by using the TSSs by default (continuous line) or the alternative TSSs (dashed line).

section 2.2.1. Note that τ has been set depending on the results from p0 and p1. This parametric case is called p2.

3.2. Out-of-pile thermal transients

A Zircaloy sample hydrogen-loaded with 254 wppm was submitted to thermal transients to assess the hydrogen precipitation/dissolution (Lacroix et al., 2018). The initial and boundary conditions were provided to the HYDCLAD model, as set in the experimental frame.

Fig. 4 shows the heating and cooling cycles to which the sample was submitted (red dashed line), together with the model-to-data comparison in terms of the dissolved hydrogen concentration evolution. The different modelling options cited above have been checked. Particularly, the results from the previous and new (with "static-TSSs") precipitation/dissolution approaches have been represented; in each case, two options of the TSSs correlations available in the model have been simulated: the option by default (McMinn's correlations for TSS_d and TSS_p) and the option that better fits to the solubility limits observed with the experimental data (Kearńs correlation for TSS_d and Zanellato's correlation for TSS_p), called alternative TSSs.

According to Fig. 4, the previous modelling of precipitation/dissolution does not capture the evolution of the dissolved hydrogen, while the new modelling follows the data trend, as was previously shown by Passelaigue et al. (2021a). The divergences of the previous modelling appear from the first cooling cycle, since the precipitation kinetics applied is too slow to simulate the precipitation observed. On the contrary, the nucleation and growth modelling for precipitation notably

enhances the prediction by capturing the observed precipitation rate after each cooling. It has been checked that there is no difference between using the previous kinetic parameter for dissolution or the new one. Furthermore, it is shown that the TSSs have an impact on the accuracy of the prediction made; indeed, the option used by default gives rise to non-negligible deviations with respect to the experimental data in the case of using the new modelling. In other words, nucleation and growth provides the right kinetics to the hydride precipitation, enabling HYDCLAD to follow data, while the alternative TSSs gives a plus to the model accuracy.

The model-to-data comparison has been also done with the new approach with "dynamic-TSSs", taking into account the alternative TSSs. The two parametric cases p0 and p1, explained in the previous section, have been simulated. Fig. 5 shows how in case of using the fitting values obtained by Passelaigue et al. (2022) (p0), slight deviations arise after the second cooling, while the same prediction as the new approach with "static-TSSs" is obtained if using bounding values of the parameters (p1). According to these results, the time parameter that characterizes the supersolubility limit decrease (τ) is the source of the differences found. In case of p0, the relatively low value of τ (lower than the duration of the experiment) leads to an earlier decrease of the supersolubility limit that gives rise to lower dissolved hydrogen after the second cooling. Thus, the way to avoid any deviation from the data evolution in this case goes through imposing a τ parameter far higher than the time of the experiment.

3.3. In-reactor irradiation

3.3.1. Non-defective fuel rod

In order to assess HYDCLAD under hydriding conditions related to hydrogen uptake in the cladding water side, a model-to-data comparison has been performed based on the post-irradiation examination (PIE) of a ZIRLO 17x17 PWR fuel rod irradiated to about 69 GWd/tU (Sahle, 2002). The measurements of two axial positions have been gathered. Table 2 shows the location and main characteristics of both locations. As observed, despite very similar oxide thicknesses, the hydrogen contents were about 40% different.
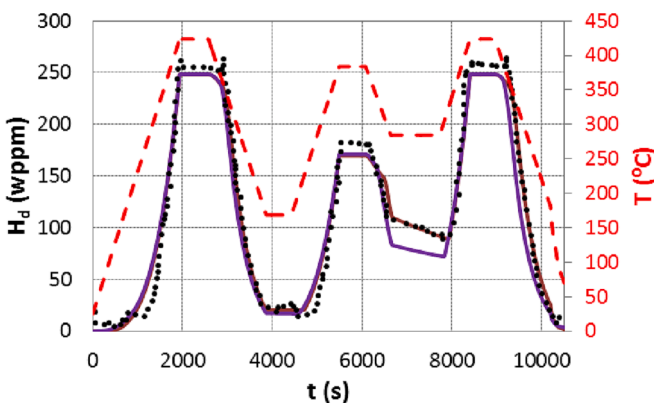

Fig. 5. Evolution during the simulated experiment of the temperature (red dashed line) and the dissolved hydrogen, both measured (black dots) and predicted with the new modelling with "dynamic-TSSs" (purple line for parametric case p0 and brown line for p1), by using the alternative TSSs.
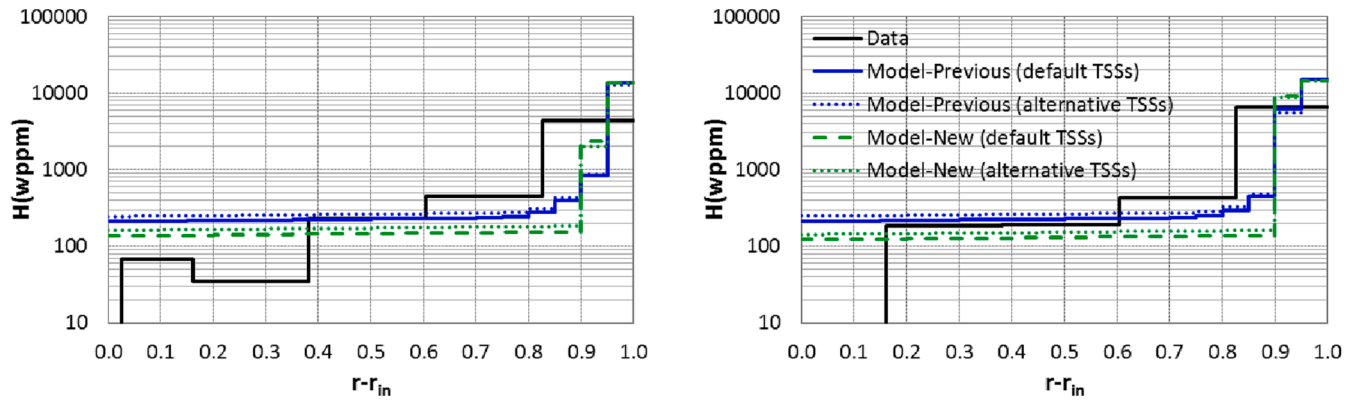
Table 2
PIE measurements (fuel fissile height, 3658 mm).

Variable	v1	v2
Axial position (mm)	2924	2925.5
Azimuth (°)	0	0
δ_{ox} (µm)	104	103
H_{pk} (wppm)*	926	1280

* Averaged through the cladding wall.

Fig. 6. Model-to-data comparison for EOL hydrogen radial distribution (normalization of the radius, r, minus the inner radius, r_{in}) for v1 (left) and v2 (right): previous vs new model ("static-TSSs") without oxidation front effect and default vs alternative TSSs.
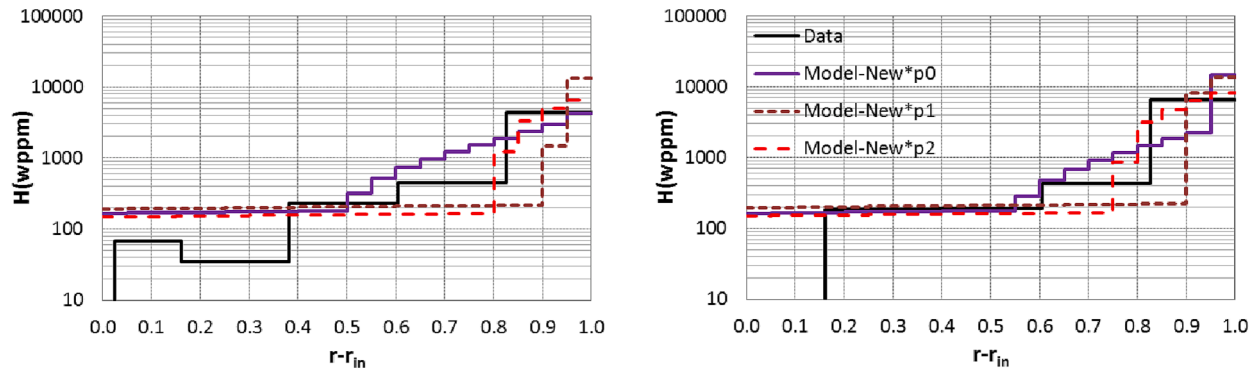

Fig. 7. Model-to-data comparison for EOL hydrogen radial distribution (normalization of the radius, r, minus the inner radius, r_{in}) for v1 (left) and v2 (right): parametric cases of new model ("dynamic-TSSs", called new*) without oxidation front effect. Alternative TSSs applied.
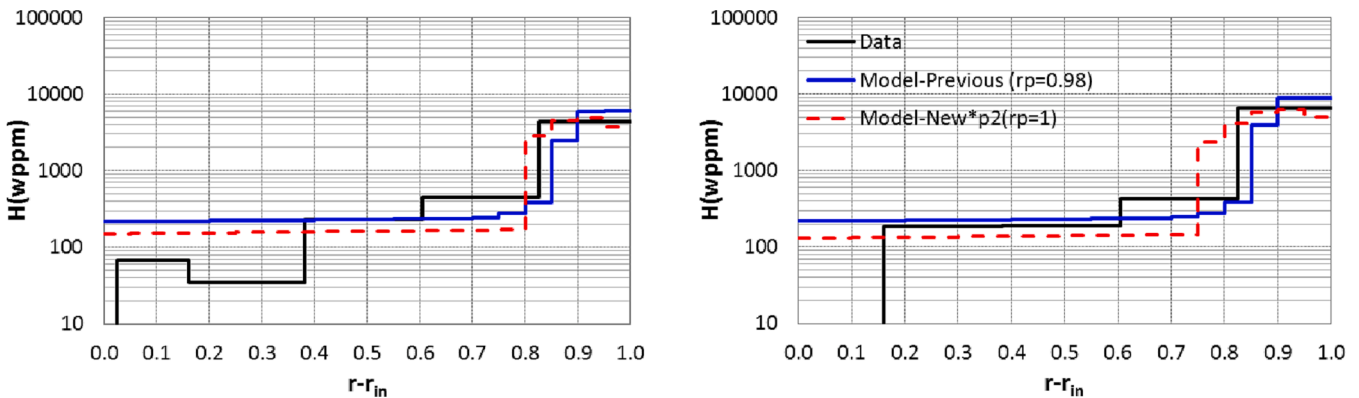

Fig. 8. Model-to-data comparison for EOL hydrogen radial distribution (normalization of the radius, r, minus the inner radius, r_{in}) for v1 (left) and v2 (right): previous model vs p2 case of new model ("dynamic-TSSs", called new*) with oxidation front effect. Alternative TSSs applied.

HYDCLAD has been coupled with FRAPCON to set the irradiation conditions, including the hydrogen pickup fraction in the cladding water side (Geelhood et al., 2015). Details of the fuel rod design and power history are given elsewhere (Feria and Herranz, 2018). Note that the oxidation rate and hydrogen pickup fraction were tuned in FRAPCON to match the δ_{ox} and H_{pk} values shown in Table 2.

Figs. 6-8 show the model-to-data comparison at end-of-life (EOL). The hydride rim measured reached 4405 wppm (v1) and 6595 wppm (v2) in the roughly 93 µm thick peripheral cladding layer. Given the relevance of the hydride rim region, the discussion below is focused on it. Nevertheless, for the rest of cladding beyond the hydride rim it might be said that the models capture the low hydride level there, which should not mean a

significant degradation of clad mechanical properties.

In order to check the impact of the extensions carried out in terms of precipitation/dissolution modelling and TSSs, Figs. 6-7 show the predictions made without the effect of the oxidation front (i.e., deactivation of the contribution). It should be highlighted:

- The new model with "static-TSSs" does not improve the prediction of the hydride rim with respect to the previous approach (Fig. 6). Both give rise to similar results in v1 and v2: important underpredictions of the rim thickness with notable overpredictions of the hydrogen concentration. The alternative TSSs does not improve the prediction;

indeed, a similar hydride rim with respect to TSSs by default is obtained.

- The new model with "dynamic-TSSs" with the best fit to out-of-pile experiments (p0 in Fig. 7) allows enlarging part of the rim thickness beyond the measurements but at the expense of giving rise to important underpredictions of the hydrogen content. Furthermore, this simulation still predicts a quite denser thin layer in the cladding water side. Therefore, it does not capture the hydride rim measured nor in v1 neither in v2. From this case, it can be observed how the decrease of the supersolubility along the irradiation (obtained through a value of τ quite lower than the irradiation period) fosters the increase of precipitated hydrides, which in turn increases the solubility limit; this allows increasing the content of dissolved hydrogen that can move inwards (responsible of the enlargement of part of the rim predicted).

- The new approach with "dynamic-TSSs" with bounding parameters values (p1 in Fig. 7) gives rise to similar predictions as the new model with "static-TSSs", that is to say, it does not overcome the inaccuracy in the hydride rim estimation. This case shows how the deactivation of the supersolubility decrease along the irradiation (through the high value of τ imposed) hinders the enlargement of the rim thickness in spite of the bounding values of the parameters related to the solubility limit (δ and g).

- In the parametric case p2 with the new approach with "dynamic-TSSs" (Fig. 7), it has been chosen the value of τ from p0 ($\tau = 10^4$ s), in order to avoid the results obtained in p1 (i.e., denser and thinner hydride rim than measured). This parametric case results in the closest prediction to the rim measured in v1 and v2. This confirms δ as a key parameter to enhance the prediction of highly hydrided regions (i.e., rim), while g does not play an important role in this regard. The prediction shows a trend to decrease the hydrogen content along the rim thickness, giving rise to a slight overprediction of this thickness (more observable in v2 due to the high hydrogen pickup).

In case of activating the oxidation front effect of HYDCLAD (Fig. 8), the parametric case p2 with the new approach with "dynamic-TSSs" enhances its prediction in terms of the hydrogen content profile in the hydride rim (the rim thickness is the same). The thickness predicted in the rim is conservative in comparison with the estimation of the previous model with the best fit of the oxidation front effect parameter, rp (also shown in Fig. 8, with a value of rp that represents a small fraction of instantaneous re-precipitation).

In the case p2 shown in Fig. 8, the rp parameter of the oxidation front contribution is set to 1 to avoid any fast re-precipitation, given that it should be reproduced through the above explained dependency with the hydride content of the precipitation kinetics related to growth (not modelled with the previous approach). However, this has resulted in a

deviation from what is expected close to the water side (lower hydrogen content estimated in the outermost layer), which would mean that the kinetics modelled is not sensitive enough to the hydride content. Anyhow, this should be checked with further validation against more PIEs made available.

Note that the stress effect on the hydrogen performance has not been modelled under irradiation conditions (mentioned above). Although this should not be a first-order effect under the conditions simulated, it could contribute to the enhancement of the model accuracy.

3.3.2. Defective fuel rod

In this case, the assessment has been focused on massive hydrogen absorption in the cladding fuel side in a Zircaloy-4 fuel rod that becomes defective at the beginning of life. As in the previous section, the coupling of HYDCLAD with FRAPCON has been used to simulate the target scenario.

A typical PWR 17x17 fuel rod irradiated to an average linear power close to 20 kW/m has been simulated with FRAPCON to obtain the beginning of life conditions; the details of rod design and irradiation are shown in Feria et al. (2020a). The study has been focused on the upper part of the fuel rod (axial zone below the upper plenum), where HYDCLAD has been applied. Particularly, a massive hydrogen pickup of 5000 wppm (in-clad average) has been modelled, as approximated observed bound from fuel rods submitted to secondary hydriding (Matsson, 2006). The beginning of this event has been simulated after 30 days of irradiation.

Figs. 9,10 represent the results obtained in terms of the precipitated hydrogen distribution across the cladding thickness. Two times after the massive hydrogen absorption have been analysed: one hour, as a representative time of the first stages of hydrogen diffusion and precipitation; and one month, as enough time for hydrogen distribution in clad to reach the steady state. A number of observations can be made from the results obtained:

- The TSSs variability does not show an important impact on the in-clad hydrides distribution, independently of the precipitation/dissolution modelling used (Fig. 9).

- The previous modelling gives rise to a rapid distribution across the whole cladding thickness of the hydrogen absorbed, even at 1 h (Fig. 9). This means that the in-clad hydrogen performance is governed by the diffusion mechanisms (related to concentration and temperature gradients), which lead to a migration rate faster than the precipitation rate.

- The new modelling results in a slower migration across the cladding thickness of the hydrogen absorbed, giving rise to localized accumulation of hydrides (Figs. 9 and 10). This is due to the faster precipitation rate simulated (through the nucleation and growth kinetic parameters), which is capable of slowing down the diffusion
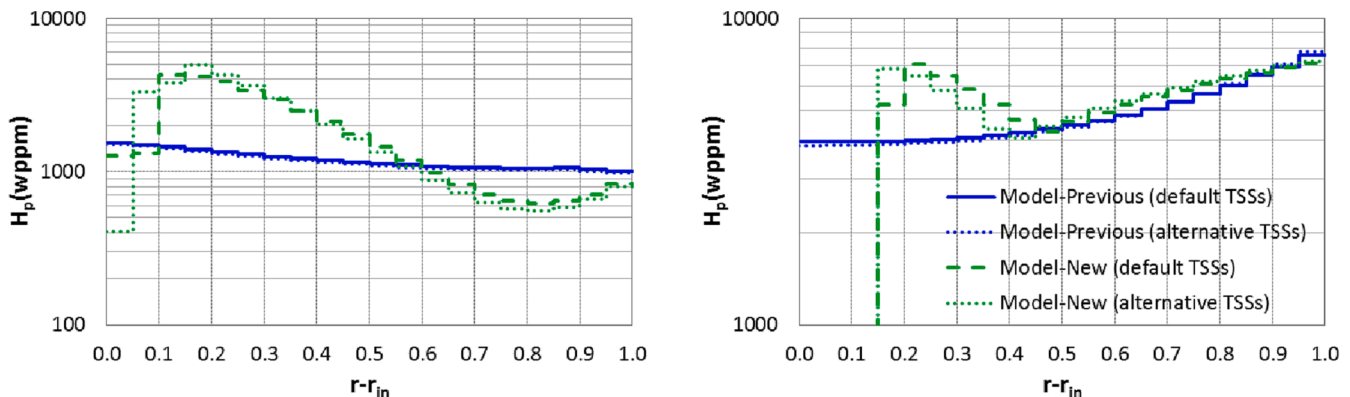

Fig. 9. Precipitated hydrogen distribution across the cladding thickness (normalization of the radius, r, minus the inner radius, r$_{in}$) at different times after the massive hydriding simulated (1 h on the left and 1 month on the right): previous vs new with "static-TSSs" model and default vs alternative TSSs.
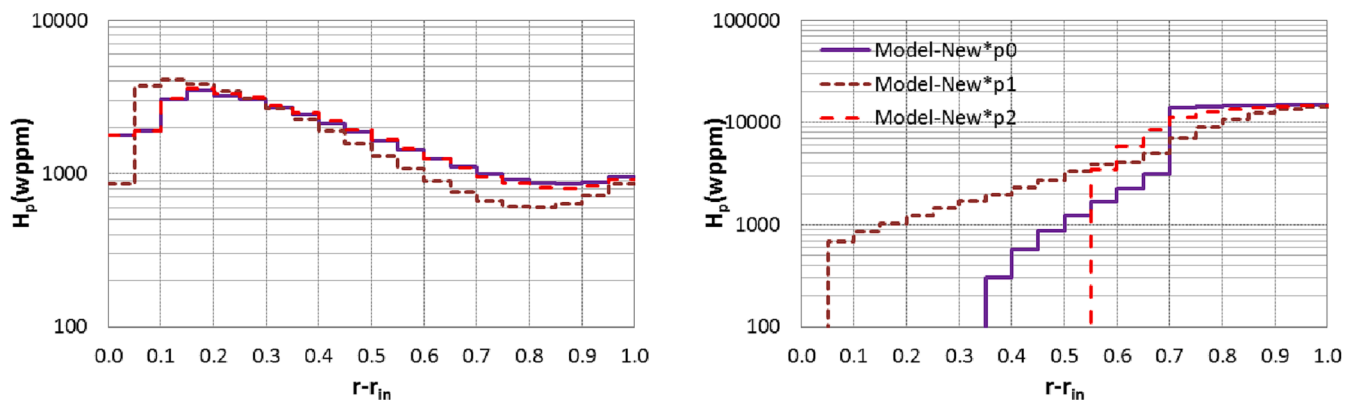
Fig. 10. Precipitated hydrogen distribution across the cladding thickness (normalization of the radius, r, minus the inner radius, r_{in}) at different times after the massive hydriding simulated (1 h on the left and 1 month on the right): parametric cases of new model with "dynamic-TSSs" (called new*). Alternative TSSs applied.

mechanisms. It has been checked that the diffusion due to the temperature gradient (i.e., Soret effect) is the responsible for the hydrides accumulation in the outer side of the cladding.

- The major differences of the parametric cases from the new approach with "dynamic-TSSs" (Fig. 10) can be observed after 1 month (figure on the right). Different extensions of the hydride rim thickness are estimated in each case; the thinner rim is predicted with the best fit to the actual irradiation scenario shown in the previous section (p2 with $\tau = 10^4$ s) and the larger rim is predicted with the bounding values of the parameters (p1). As mentioned above, the high value of τ in the case p1 deactivates the supersolubility decrease, which enlarges the rim thickness in this scenario.

From the above discussion, it was highlighted that the new approach is capable of predicting hydrides distribution expected in secondary hydriding scenarios, where the formation of blisters is observed (Evdokimov et al., 2011; Lee et al., 2017). However, the lack of data in this regard prevents from validating the parametric cases of the new approach with "dynamic-TSSs".

4. Conclusions

The present work is focused on analysing the impact of hydrogen precipitation modelling on hydrides distribution across the cladding. Two scenarios have been addressed: hydriding in non-defective fuel rods (from a progressive hydrogen pickup in the cladding water side) and secondary hydriding in defective fuel rods (from a massive pickup in the cladding fuel side). Particular attention has been given to the potential effect of a more phenomenological approach (based on nucleation and growth) to the previous precipitation/dissolution modelling; likewise, several solubility limits have been explored to know the modelling sensitivity to the scatter in the existing database. All the studies have been carried out with HYDCLAD, an in-house model addressing hydrogen performance in the cladding.

The results obtained allow drawing the following conclusions:

- The more phenomenological approach is capable of notably enhancing the prediction made under representative irradiation of non-defective cladding. Nonetheless, it is worth noting that this enhancement comes along with a model re-parametrization with respect to previous settings, and the consideration of the oxidation front effect, especially in the hydride rim prediction (based on assessment against PIEs). The wide variability of TSSs, though, hardly has an effect.
- The enhancement of nucleation and growth modelling would strongly affect hydrides distribution in secondary hydriding scenarios, being capable of estimating the hydrides blisters expected.

Contrarily, in-clad hydrides distribution is hardly sensitive to TSSs variability.

To sum up, by a suitable re-parametrization of the new nucleation and growth model and the consideration of the "push effect" of the oxidation front, a substantially better description of hydrides distribution across cladding can be achieved, particularly with HYDCLAD. The cited re-parametrization has been required in this work due to the fact that the related modelling of previous work needed further assessment under representative irradiation conditions; the different parameters values obtained in the present paper confirm the need of carrying out the assessment against expected fuel rod scenarios. Thus, this work will be further supported once more data become available in the open literature.

CRediT authorship contribution statement

F. Feria: Conceptualization, Investigation, Methodology, Software, Writing – original draft. **L.E. Herranz:** Conceptualization, Investigation, Writing – review & editing.

Declaration of Competing Interest

The authors declare that they have no known competing financial interests or personal relationships that could have appeared to influence the work reported in this paper.

Data availability

Data will be made available on request.

References

Avrami, M., 1939. Kinetics of Phase Change. I General Theory. The Journal of Chemical Physics 7, 1103–1112.

Bruni, G., Lewis, B.J., Thompson, W.T., 2011. Framework model for hydrogen redistribution in Zircaloy sheathing. J. Nucl. Mater. 409, 33.

Courty, O.F., Motta, A.T., Hales, J.D., 2014. Modeling and simulation of hydrogen behavior in Zircaloy-4 fuel Cladding. J. Nucl. Mater. 452, 311–320.

Courty, O.F., Motta, A.T., Piotrowski, C.J., Almer, J.D., 2015. Hydride precipitation kinetics in Zircaloy-4 studied using synchrotron X-ray diffraction. J. Nucl. Mater. 461, 180–185.

Evdokimov, I.A., Likhanskii, V.V., Aliev, T.N., Sorokin, A.A., Kanukova, V.D., 2011. Secondary hydriding criteria under irradiation conditions. Nucl. Eng. Des. 241 (5), 1414–1420.

Feria, F., Herranz, L.E., 2018. Effect of the oxidation front penetration on in-clad hydrogen migration. J. Nucl. Mater. 500, 349–360.

Feria, F., Aguado, C., Herranz, L.E., 2020a. Methodology for a realistically conservative characterization of spent fuel in dry storage. Ann. Nucl. Energy 140, 107148.

Feria, F., Aguado, C., Herranz, L.E., 2020b. Extension of FRAPCON-xt to hydride radial reorientation in dry storage. Ann. Nucl. Energy 145, 107559.

Geelhood, K.J., Luscher, W.G., Raynaud, P.A., Porter, I.E., 2015. FRAPCON-4.0: A Computer Code for the Calculation of Steady-State, Thermal-Mechanical Behavior of Oxide Fuel Rods for High Burnup. PNNL-19418 Vol. 1 Rev, 2.

Kammenzind, B., Franklin, D.G., Peters, H.R., Duffin, W.J., 1997. Hydrogen pickup and redistribution in alpha-annealed Zircaloy-4. In: in: 11th International Symposium on Zirconium in the Nuclear Industry. ASTM STP1295, pp. 338–369.

Kearns, J.J., 1967. Terminal solubility and partitioning of hydrogen in the alpha phase of zirconium, zircaloy-2 and zircaloy-4. J. Nucl. Mater. 22, 292–303.

Lacroix, E., Motta, A., Almer, J., 2018. Experimental determination of zirconium hydride precipitation and dissolution in zirconium alloy. J. Nucl. Mater. 509, 162–167.

Lee, J.-M., Kook, D.-H., Cho, I.-J., Kim, Y.-S., 2017. A study on the reaction of Zircaloy-4 tube with hydrogen/steam Mixture. J. Nucl. Mater. 491, 105–114.

Marino, G.P., 1972. A numerical calculation of the redistribution of an interstitial solute in a thermal gradient. Nucl. Sci. Eng. 49, 93–98.

Massih, A.R., Jernkvist, L.O., 2009. Stress orientation of second-phase in alloys: Hydrides in zirconium alloys. Comput. Mater. Sci 46, 1091.

Matsson, I., 2006. Studies of Nuclear Fuel Performance Using On-site Gamma-ray Spectroscopy and In-pile Measurements. Dissertation presented at Uppsala University, ISBN 91-554-6582-X.

McMinn, A., Darby, E.C., Schofield, J.S., 2000. The terminal solid solubility of hydrogen in zirconium alloys. In: 12th Int. Symp. On Zr in the Nuclear Industry, Toronto, CA, pp. 173–195.

Nagase, H., Uetsuka, F., 1997. Hydride morphology and hydrogen embrittlement of Zircaloy fuel cladding used in NSRR/HBO experiment, in: ANS Int. Top. Meet. Light Water React. Performance, ANS, Portland, OR, p. 677.

Passelaigue, F., Lacroix, E., Pastore, G., Motta, A.T., 2021a. Implementation and Validation of the Hydride Nucleation-Growth-Dissolution (HNGD) model in BISON. J. Nucl. Mater. 544, 152683.

Passelaigue, F., Simon, P.-C.-A., Motta, A.T., 2021b. Modified_HNGD_Validation. Mendeley Data v1. https://doi.org/10.17632/6ftsfyfpbz.1.

Passelaigue, F., Simon, P.-C.-A., Motta, A.T., 2022. Predicting the hydride rim by improving the solubility limits in the Hydride Nucleation-Growth-Dissolution (HNGD) model. J. Nucl. Mater. 558, 153363.

Sahle, W., 2002. PIE of CIP0-1 Father Rod: Cladding oxide and hydride measurements in SEM. Studsvik Report N(H)-02/027.

Sawatzky, A., 1960. Hydrogen in Zircaloy-2: Its distribution and heat of transport. J. Nucl. Mater. 2, 321–328.

Sonnenburg, H.G., Boldt, F., 2017. Brennstabverhalten im Normalbetrieb, bei Störfällen und bei Langzeitlagerung. GRS-Bericht: GRS – 464, ISBN 978-3-946607-47-2.

Stafford, D.S., 2015. Multidimensional simulations of hydrides during fuel rod lifecycle. J. Nucl. Mater. 466, 362–372.

Szabó, P., Hózer, Z., 2019. Hydrogen uptake tests with zirconium alloys at reactor operational temperatures. Tech. Rep. EK-2021-437-1-1-M0.

Tupin, M., Bisor, C., Bossis, P., Chêne, J., Bechade, J.L., Jomard, F., 2015. Mechanism of corrosion of zirconium hydride and impact of precipitated hydrides on the Zirclaoy-4 corrosion behavior. Corros. Sci. 98, 478–493.

Une, K., Ishimoto, S., Etoh, Y., Ito, K., Ogata, K., Baba, T., Kamimura, K., Kobayashi, Y., 2009. The terminal solid solubility of hydrogen in irradiated Zircaloy-2 and microscopic modeling of hydride behavior. J. Nucl. Mater. 389, 127–136.

Veshchunov, M.S., Shestak, V.E., Ozrin, V.D., 2016. A new model of hydrogen redistribution in Zr alloy claddings during waterside corrosion in a temperature gradient. J. Nucl. Mater. 472, 65–75.

Zanellato, O., Preuss, M., Buffiere, J.Y., Ribeiro, F., Steuwer, A., Desquines, J., Andrieux, J., Krebs, B., 2012. Synchrotron diffraction study of dissolution and precipitation kinetics of hydrides in Zircaloy-4. J. Nucl. Mater. 420, 537–547.